THE LANCET
Microbe

Supplementary appendix

This appendix formed part of the original submission and has been peer reviewed. We post it as supplied by the authors.

Supplement to: Schurink B, Roos E, Radonic T, et al. Viral presence and immunopathology in patients with lethal COVID-19: a prospective autopsy cohort study. *Lancet Microbe* 2020; published online September 25. https://doi.org/10.1016/S2666-5247(20)30144-0.

Supplementary material

1. Methods

1.1 Supplementary Table 1 sampling locations

1.2 Supplementary Table 2 stains and dilutions

1.3 Staining protocols

1.4 Supplementary Table 3, baseline characteristics per treatment location

1.5 Table 4: definitions used in histology

2. Results

2.1 Supplementary Table 4, SARS-CoV2 antibody positivity

2.2 Histopathological descriptions

2.3 Supplementary Figure 1, cardiac histology

2.4 Supplementary Figure 2, other organ histology

Supplementary Methods

1.1 Table 1: sampling locations

Respiratory tract	▪ Trachea ▪ Upper airway ▪ Lungs: all lobes central and peripheral tissue
Heart	▪ Atria ▪ Ventricles ▪ Septum
Digestive tract	▪ Oesophagus ▪ Stomach ▪ Duodenum ▪ Ileocecal ▪ Pancreas ▪ Liver
Urogenital tract	▪ Kidneys ▪ Bladder ▪ Prostate ▪ Uterus
Miscellaneous	▪ Femoral nerve ▪ Omental fat ▪ Mesenteric fat ▪ M. Quadriceps ▪ Lymph nodes ▪ Submandibular glands
Brain	▪ All cerebral lobes ▪ Hypothalamus ▪ Hippocampus ▪ Neostriatum ▪ Thalamus ▪ Amygdala ▪ Pineal gland/epiphysis cerebri ▪ Meninges ▪ Cerebellum ▪ Medulla oblongata ▪ Pons ▪ Mesencephalon ▪ Cervical spinal cord

1.2 Table 2: stains and dilutions

Antibody	Firm	Clone	Species	Catalogue number	IVD/RUO	Expr1	Ventana Ultra Validated dilution	Ventana Ultra Validated incubation time
C3d	Agilent/Dako	A0063	Rabbit	A063	CE-IVD	24 min CC1	1/1000	32 min
CD003	Agilent/Dako	polycl	Rabbit	A0452	CE-IVD	24 min CC1	1/150	32 min
CD004	Abcam	SP35	Rabbit	ab213215	CE-IVD	32 min CC1	1/50	48 min
CD008	Dako	144B	Mouse	M7103	CE-IVD	32 min CC1	1/50	32 min
CD020cy	Dako	L26	Mouse	M0755	CD-IVD	24 min CC1	1/500	16 min
CD031	Agilent/Dako	JC70A	Mouse	M0823	CE-IVD	24 min CC1	1/100	32 min
CD045	Agilent/Dako	2B11+PD7/26	Mouse	M0701	CE-IVD	24 min CC1	1/100	32 min
CD061	Dako	Y2/51	Mouse	M0753	CE-IVD	24 min CC1	1/25	64 min
CD068	Agilent/Dako	KP1	Mouse	M0814	CE-IVD	24 min CC1	1/10000	32 min
GLUT-1	Thermo scientific	polycl	Rabbit	RB-9052-P	CE-IVD	24 min CC1	1/200	32 min
Ker 007	Dako	OVTL12/30	Mouse	M7018	CE-IVD	32 min CC1	1/100	32 min
MPO (cardiac)	Dako	polycl	Rabbit	A0398	CE-IVD	24 min CC1	1/8.000	32 min
MPO (neutrophils)	Dako	Polycl	Rabbit	A0398	CE-IVD	20 min CC1	1/10000	4°C overnight
CitH3	Abcam	Polycl	Rabbit	ab5103	CE-IVD	10 min CC1	1/1000	60 min R.T
Fibrinogen	Dako	Polycl	Rabbit	F0111	CE-IVD	24 min CC1	1/100	32 min
MBP	Chemicon	84-89	Mouse	MAB387	CE-IVD	-	1/50	64 min
Granzym B	Monosan	GrB-7	Mouse	MON 7029C	CE-IVD	32 min CC1	1/300	48 min
HLA-DR (LN3)	Monosan	LN-3	Mouse	MON 1081	CE-IVD	24 min CC1	1/300	32 min
GFAP	Dako	Polycl	Rabbit	Z0334	CE-IVD	24 min CC1	1/16000	16 min
PAS								
Schiff	Merck			1.09033.0500				
Hematoxyline	Mayer			N/A				
Periodic Acid	Sigma-Aldrich			10450-60-9				
Ethanol	-			64-17-5				
Xylene	-			1330-20-7				
α-amylase porcine pancreas	-	N/A	N/A	9000-90-2	CE-IVD	98 min	N/A	

1.3 Staining

Protocol optimization SARSCoV2 stains

Formalin-fixed paraffin-embedded (FFPE) samples of all organs were evaluated for the distribution of SARS-CoV2 in a subset of patients. Viral antigen was localized by two antibodies directed against the SARS CoV2 nucleocapsid protein: a monoclonal mouse antibody (clone 46-4, kindly provided by Erik Snijders, LUMC Leiden, the Netherlands) and a second polyclonal rabbit antibody (catno.40143-T62 Sino Biological inc). Both antibodies were validated on FFPE sections of SARS CoV2 infected and SARS CoV2 negative VeroE6 cells in suspension, which were fixed with 4% formaldehyde and paraffin-embedded (Supplementary figure). Further validation was performed by staining tissues of SARS-CoV2 negative patients (positive for Influenza A) and FFPE sections that were RT-PCR proven positive for SARS CoV2. The optimal protocol for the monoclonal mouse antibody was pretreatment with CC1 for 32 minutes at a dilution of 1:10.000 incubated at 36°C for 64 minutes. The optimal protocol for the polyclonal rabbit antibody was pretreatment with CC1 for 24 minutes at a dilution of 1:75.000 incubated at 36°C for 32 minutes. FFPE sections of all organs were stained in the Ventana Benchmark Ultra, Optiview detection kit with DAB and CuSO4. Lungs were processed for EM, but were negative for viral particles. Post-mortem real-time PCR of SARS-CoV2 was executed using bronchus and nasopharyngeal swabs and lung biopsies on all patients. To minimize contamination, samples were collected at the beginning of the autopsy. Lung FFPE sections were tested for SARS-CoV2 using RT-PCR on FFPE tissue to ensure proper validation of the antibody. The samples with major presence of virus as determined immunohistochemically were positive (n=2) with RT-PCR, while those with sporadic presence of infected cells were negative or of too low quality (n=9). Since RT-PCR results were possibly negatively influenced by postmortem tissue quality and were often deemed of too little quality, it is not further elaborated in the paper.

Protocol Neutrophils

To visualize NETosis, FFPE sections from various tissues were stained for myeloperoxidase (MPO; rabbit anti-human pAb, Dako A0398, 1:10,000) and citrullinated histone 3 (CitH3; rabbit anti-human pAb, Abcam ab5103, 1:1000), whereas consecutive samples were stained with hematoxylin/eosin (HE; Klinipath, Amsterdam, The Netherlands) to determine localization of the extracellular DNA traps.

1.4 Table 3. Baseline characteristics of both locations

Baseline characteristics per center	Location #1 (n=10)	Location #2 (n=10)	P-value
Age (Median, range)	66 (60-78)	72 (41-78)	0.42
Sex (Male/Female)	7/3	8/2	0.74
Comorbidity	9	7	0.11
Duration of illness	24 (13-31)	20 (5-44)	0.42
Renal failure	8	7	0.61
Cardiac symptoms	7	6	0.48
Thromboembolic events	6	3	0.23
Neurological symptoms	5	5	0.93
Supra-infection	6	3	0.23

Supplementary Table 3. Baseline characteristics for both treatment locations. These data were not significant. On one patient autopsy was performed at location #2, however he was treated elsewhere and is therefore not included in this table.

1.5 Table 4. Clinical and histological definitions

Condition	Definition	Reference
Histology		
Heart: Myocarditis	An inflammatory infiltrates within the myocardium associated with myocyte degeneration and necrosis of non-ischemic origin. The inflammatory infiltrate should consist of ≥14 leucocytes/mm^2 including up to 4 monocytes/mm^2 with the presence of CD3 positive lymphocytes ≥7 cells/mm^2	Dallas criteria , Caforio et al. (2013)
Liver: Portal inflammation, lobular inflammation and interface activity	minor (grade 1), moderate (grade 2) or severe (3).	
Liver: Bile duct damage, ballooning and thrombi	were evaluated (absent/present)	
Liver: Steatosis	grade 0 (< 5%), grade 1 (5-33%), grade 2 (33-66%) or grade 3 (>66%).	
Liver: Confluent parenchymal necrosis	%	
Liver: Grade of fibrosis	(0) none, (1) perisinusoidal and/or periportal, (2) bridging fibrosis, involving less than 50% of the portal tracts and/or central veins, (3) bridging fibrosis, involving more than 50% of the portal tracts and/or central veins (4) cirrhosis.	
Clinical		
Disease course	Time between first symptoms and time of death in days	
Renal failure	Acute kidney injury stages: I: SCr 1.5-1.9 times baseline or ≥0.3 mg/dl increase + urine output <0.5mg/kg/h for 6-12h II: SCr 2.0-2.9 times baseline + urine output <0.5mg/kg/h for ≥12h III: SCr 3 times baseline or increase in SCr to ≥4 mg/dl or initiation of renal replacement therapy + urine output <0.3mg/kg/h for ≥24h or anuria for ≥12h	KDIGO Clinical Practice Guideline for acute kidney injury
High dose steroids	>10mg prednisone or >40 mg hydrocortisone per day	
Thromboembolic events Pulmonary embolism	Score >4 of the Wells criteria or based on CT	

Supplementary Results

2.1 Supplementary Table 5

Supplementary Table 5. SARS-CoV2 staining per patient														
	Length of Illness	Lung	Heart	Brain	Lower GI tract	Upper GI tract	Major airways	Salivary glands	Kidney	Liver	Pancreas	Spleen	Bone marrow	Adipose tissue
1	5	Yes	No	No	No	Yes	-	-	No	Yes	No	No	No	No
2	27	No	No	No	No	No	No	-	No	No	No	No	Yes	No
3	22	Yes	No	No	No	No	No	-	No	No	No	No	-	No
4	12	No	No	No	No	No	No	Yes	No	No	No	No	No	No
5	17	Yes	No	No	No	No	No	Yes	No	No	No	No	No	No
6	10	Yes	Yes	No	No	Yes	No	No	No	No	Yes	No	No	Yes (omentum)
7	8	Yes	No	No	Yes	No	Yes	Yes	Yes	No	No	No	-	No
8	6	Yes	Yes	No	No	No	Yes	No	No	No	No	No	No	No
9	24	Yes	No	No	No	No	No	No	No	Yes	Yes	Yes	No	Yes (omentum and mesocolic fat)
10	44	No	Yes	No	No	No	No	No	No	No	No	No	-	No
11	31	Yes	No	No	No	No	No	No	No	No	No	No	No	No

Supplementary Table 5. Positive SARS-CoV2 antibody per organ per patient. The staining was deemed positive if both antibodies used stained the same cell type.

2.2 Histopathological descriptions

Heart

Transmural sections of each heart (n=20) were taken from the left ventricle (LV) and right ventricle (RV). Pre-existent pathological changes were mild in all cases, and consisted of mild myocardial hypertrophy in most cases, and focal patchy or interstitial fibrosis (LV: 6 out of 20 hearts, RV: 7 out of 20 hearts). In contrast, acute pathological changes were observed in all 20 hearts, and consisted of interstitial edema, and inflammatory cell infiltrations which were mostly histiocytic (CD68+, CD45+) in all cases with variable admixture of T lymphocytes (CD3+) and/or PMN (MPO+). The infiltrates were found in either endocardium, myocardium, epicardial fat or in combinations of them. In detail: epicarditis and endocarditis composed of lymphohistiocytic infiltrations were found in all hearts. Myocarditis characterized by presence of large numbers of histiocytes and small focal or diffuse infiltrations of T-cells were found in 11/20 hearts, combinations of histiocytes and PMN were found in 9/20 hearts. Myocyte injury, either as small clusters or individual cells identified by means of cytoplasmic positive C3d immunostaining was present in nearly all cases either as isolated cells or grouped cells (LV: 20/20; RV: 12/20 hearts). In addition, fibrin platelet thrombi were noticed in the small intramyocardial blood vessels, and confirmed by CD31+ immunostaining (LV: 10/20; RV: 8/20 hearts). Small endocardial mural thrombi were present in 3 out of 21 hearts.

Liver

In the 21 livers studied, 11 patients had (50%) steatosis, 10 patients grade 1 (5-33%) and one patient grade 2 steatosis (35%). No convincing steatohepatitis was seen in any patient. Minor portal inflammation was present in 13 patients and minor lobular inflammation in 6 patients. Interface activity did not occur. Bile duct lesions were not present in most of the specimens; only 1 patient showed subtle lymphocytic cholangitis or bile duct irregularity. Fibrosis was seen in 11 patients of whom 8 showed some periportal and/or perisinusoidal fibrosis and 3 patients true bridging (14%), probably due to pre-existing liver damage. In one patient, extensive iron was seen in hepatocytes (grade 4) as co-incidental finding. In 5 patients confluent necrosis occurred, ranging from 5-50%. In only one patient, a potential thrombus in small artery was seen (without additional staining to increase sensitivity).

Spleen

The mean weight of the spleens that were investigated was 237 g with a range of 100 to 326 g. The spleens showed normal architecture of white and red pulp, no remarkable lymphoid hyperplasia was present (CD20, CD3). 15 out of 19 spleens showed congestion. Almost all the spleens showed presence of neutrophils in the red pulp, some with neutrophil plugs in the vessels (MPO). Some spleens showed a tremendous number of thrombocytes and dense aggregates of thrombocytes (CD61) in the red pulp. In only one case there was suspicion of haemophagocytosis (CD68).

In conclusion: most spleen showed signs of acute splenitis sometimes with plugs of neutrophils in the splenic vessels, but no signs of thrombosis. Furthermore, a tremendous amount of thrombocytes and their aggregates were found in the red pulp.

Bone marrow

Trilinear hyperplasia of haematopoeietic cell lineages was constant finding in almost all bone marrow samples (n=12/15). The most striking feature was the increase of megakaryocytes (CD61) (n=12/15). The megakaryocytes were not only increased in number but also showed marked deviation in shape. In almost all the marrow samples a part of the megakaryocytes showed enlargement and hyperlobulation with sometimes “stag-horn” formation of the nucleus (n=11/15). There was a tendency to form loose clusters (n=4/15). Most bone marrow samples showed signs of fibrosis grade 1 (Gomorri) (n=6/15).

Kidney

All cases showed signs of circulatory dysfunction, consisting of congestion of glomeruli and peritubular capillaries. One case showed medullary interstitial hemorrhage. Although these are well known features of generalized activation of coagulation, in 20/21 patients no convincing microthrombi were found in the glomerular or peritubular capillaries. One case showed signs of endothelial activation, characterized by mild endothelial swelling and arteriolar sequestration of leukocytes. No specific glomerular cell changes were found, apart from pre-existent glomerular sclerosis or signs of glomerular ischemia.

All cases showed moderate to severe signs of acute tubular injury, consisting of tubular dilation, simplification of tubular epithelial cells (TEC) and loss of the TEC brush borders, most prominent in the corticomedullary

transition zones. Two thirds of cases showed a striking vacuolization of TEC in the proximal tubules, which seems to be characteristic for COVID-19 infections, as this is usually not encountered in cases of acute tubular necrosis in the context of post-mortem autolytic changes. One case showed strikingly extensive tubular oxalosis. Approximately half of the cases showed a variety of pre-existent chronic damage, partly related to ageing, such as arteriosclerosis, arteriolar hyalinosis, and varying degrees of interstitial fibrosis and tubular atrophy.

Brain

Macroscopically, most brains were normal with thin transparent meninges and on cut no signs of atrophy , hemorrhages or infarction. The brain of one patient with a pre-existing acute necrotizing encephalopathy showed necrosis in the region of the basal nuclei and capsules and in the rostral part of the brainstem. Atrophy of the hippocampus and amygdala was noted in another patient with dementia of Alzheimer type.

Histologic examination showed similar findings in all patients. Both white and gray matter were affected. All presented moderate to severe activation of microglia, with cells showing an ameboid or frankly macrophagic morphology. In the more severe cases, microglia clustered in nodules. This was associated with loose perivascular cuffings of T lymphocytes. Sparse T lymphocytes were also noted in the parenchyma. These lymphocytes were CD4-predominant in most cases, whereas in few CD8-positive cells were more represented. These lymphocytes were only sporadically Granzyme-B positive. No B lymphocytes were present, and no loss of myelin or bleedings occurred. A mild to moderate isomorphic reactive astrogliosis was always noted. These findings were more severe in the cranial medulla oblongata and in the olfactory bulb, but also present in all other regions examined, including the frontal cortex and white matter, chiasma, hippocampus, neostriatum, cerebellum and spinal cord.

Neutrophils

In lung tissue, neutrophils were distributed throughout, either as single cells or aggregates, many still containing their cytoplasmic granules, but there were also areas with cell-free MPO-containing granules and released MPO (areas with red/pinkish staining). CitH3 was seen in all sections, although the intensities varied between patients, with faint to pronounced staining of nuclei, until this typical DNA trap patterns often associated with intense MPO staining.

Comparison of these markers in various organs was with decreasing intensity, most intense in lung and then liver, heart and brain. In liver there was less citH3, predominantly associated with swollen nuclei, whereas released MPO was most intense compared to any of the other organs. However, in some sections DNA traps were found with aggregated neutrophils and citH3 (SVU20-41-I). In the heart both MPO and citH3 staining was apparent, although only in one patient (SVU20-45-F) we did see pronounced DNA traps. In brain tissue we found some scattered neutrophils staining for citH3 and a considerable number of citH3-positive nuclei not associated with MPO in grey matter and not in white matter. In blood vessels in the brain we found aggregated neutrophils staining citH3 positive. Typical DNA trap structures were not seen. We also analyzed a major thrombus in the bronchus of one of the patients where we found intense granular and released MPO staining combined with marked citH3 staining with the occasional staining pattern of DNA traps.

2.3 Supplementary Figure 1: Cardiac histopathology

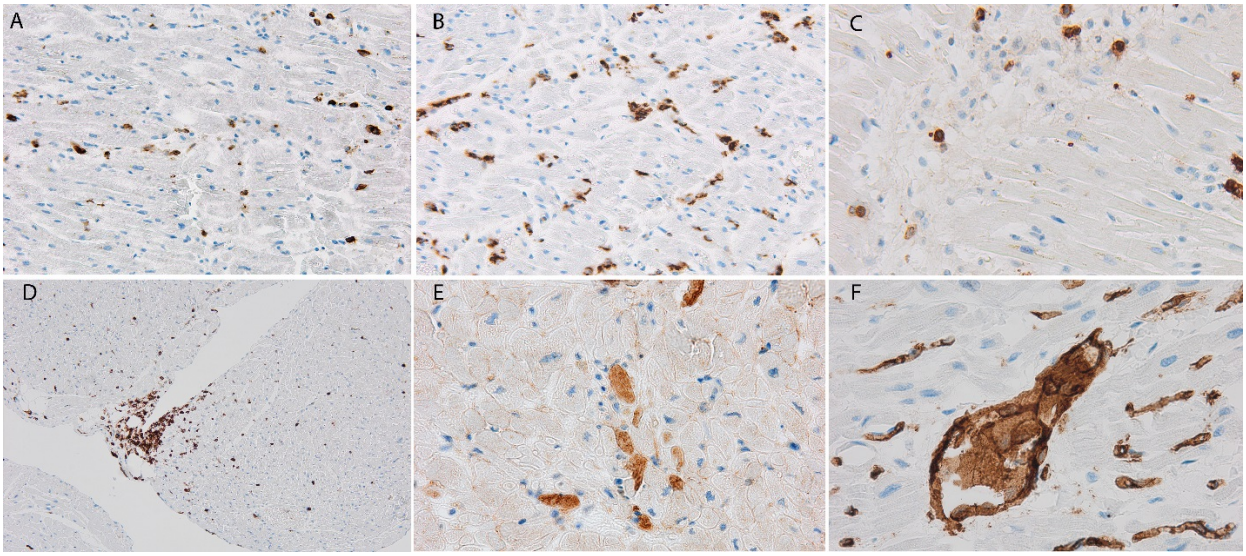

Figure 1: composite panel of immune stained sections illustrating the distinct inflammatory and thrombotic changes of the heart in COVID-19 patients. Brown stained cells in all panels represent the cells that stain positively with the respectively applied antibodies. Fig 1A-C: detail of myocardium in 3 serial sections showing inflammatory infiltrates composed of macrophages. A) CD45 stain, subpopulation of macrophages; B) CD68 stain, pan macrophage marker) C) To a lesser extent T-lymphocytes. (CD3 stain). D) Detail of endomyocardium showing distinct sub endocardial cluster of T lymphocytes directly underneath the endocardial layer of the heart, and diffuse presence of T-lymphocytes in the adjacent myocardium. E) Detail of myocardium showing myocyte injury, appearing as individual death cells showing diffuse brown cytoplasmic staining with a complement factor C3d antibody. F) detail of myocardium stained with CD31 antibody, reactive with both endothelial cells and platelets, showing multiple brown stained capillaries and a centrally located hugely dilated micro vessel containing an occluding fibrin platelet thrombus.

2.4 Supplementary Figure 2: other organ histology

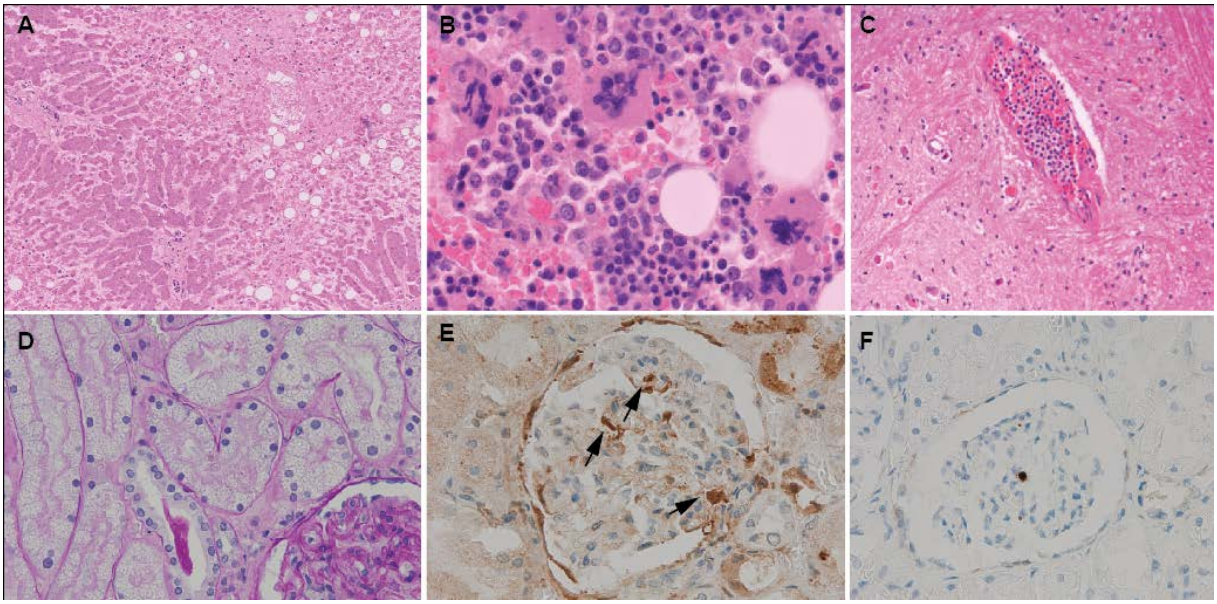

Supplementary figure 2. Histopathology of extra-pulmonary organs. A) hematoxylin and eosin (H&E) stain of the liver shows mild macrovesicular steatosis and a few inflammatory cells in the portal fields. The liver architecture is preserved. Magnification 100x B) H&E stain of the bone marrow reveals trilinear hyperplasia and presence of clustered and dysmorphic megakaryocytes with hyperlobulated nuclei. Magnification 400x C) H&E stain of the medulla oblongata in the brain shows a plug of neutrophils in a middle size arteriole. Magnification 200x D) Periodic acid Shiff (PAS) stain of the kidney shows diffuse fine vacuolization of the cytoplasm of the distal tubular epithelial cells. Magnification 400x E) stain against fibrinogen of the kidney shows presence of fibrin microthrombi in the capillary of a glomerulus (arrows). F) stain against CD61 of the kidney reveals that the microthrombi also contain platelets. Magnification 400x.